Physical Performance Evaluation of the Toshiba GCA-9300A Triple-Headed System

Kypros Kouris, Gillian A. Clarke, Peter H. Jarritt, Caroline E. Townsend and Shane N. Thomas

Institute of Nuclear Medicine, University College and Middlesex School of Medicine, London, United Kingdom

The physical performance of the Toshiba GCA-9300A triple-headed SPECT system has been assessed. Using a water-filled cylinder containing ^{99m}Tc, the tomographic volume sensitivity was 33.8 and 34.8 kcps/(MBq/ml)/cm for the high-resolution, parallel-hole (HR-PH) collimator and the super high-resolution, lead fanbeam (SHR-FB) collimator, respectively, excluding the rotation time(s) during scanning when data are not acquired. The tomographic spatial resolution at the center, in air, with 132 mm radius of rotation was 10.2 and 7.8 mm FWHM with the HR-PH and SHR-FB collimators, respectively; in water it was 11.0 and 7.8 mm. Reconstructed relative activity concentrations were accurate for both collimator sets if attenuation correction was used. With the SHR-FB collimators, the average peak-to-valley ratio of five-line sources in water improved significantly when an asymmetric energy window was used. Using the three-dimensional Hoffman brain phantom which simulates a 4:1 grey matter-to-white matter ratio and the usual choice of acquisition and processing parameters for brain studies, the reconstructed grey matter-to-white matter ratio was only about 1.7 for total counts typically acquired in a ^{99m}Tc-HMPAO study (4.0 M counts) and only 2.3 for 40 M counts. There was a qualitative improvement with an asymmetric energy window.

J Nucl Med 1993; 34:1778–1789

The role of single photon emission computed tomography (SPECT) in clinical practice and research has been enhanced with the introduction of multiheaded but primarily triple-headed systems (*1–3*). Compared to a conventional single rotating gamma camera, they can yield superior image quality (*4*) even at lower patient doses and/or lower acquisition times (*5*) due to increased tomographic volume sensitivity and improved spatial resolution. With parallel-hole collimators, some of the gain in sensitivity can be traded-off for improved resolution using narrower holes and/or increased hole length. Because of the properties of fanbeam collimators, both sensitivity and resolution can improve (*6–8*). Thus, SPECT protocols can now be tailored to the clinical problem. The pertinent variables are the amount of activity administered, collimator choice and total data acquisition time.

In this paper, we present the physical performance assessment of the Toshiba GCA-9300A (Toshiba Corporation, Tokyo, Japan), a triple-headed system for head and body SPECT. Where appropriate, comparison is made with the performance of the GE/CGR Neurocam (General Electric Medical Systems, Milwaukee, WI), a brain-dedicated, triple-headed system, previously evaluated at our institution (*5,9*).

MATERIALS AND METHODS

Toshiba GCA-9300A

The Toshiba GCA-9300A is a triple-headed multislice SPECT system for both brain and body tomography (*2*). It consists of three Anger-type gamma cameras forming a triangular aperture in a rotating gantry. The radius of rotation of each camera can be varied independently between 132 and 307 mm. Each camera has 45 photomultiplier tubes (PMTs) coupled to a 6.5-mm thick NaI(Tl) crystal and is shielded against gamma rays and x-rays up to 180 keV. The collimators can be changed using custom trolleys. The collimators available at our institution are the high-resolution, parallel-hole (HR-PH) and the super high-resolution fanbeam (SHR-FB) both cast from lead. The fields-of-view (FOV) are 410 mm × 210 mm with the parallel-hole collimators, and 220 mm × 210 mm with the fanbeam collimators. The fanbeam collimators have a focal length of 397 mm and must be used with the minimum radius of rotation (132 mm).

Tomographic data can be acquired in either the 'step and shoot' or 'continuous rotation' mode. In the latter, more than one rotation can be performed with the rotation direction reversing between rotations. Data from each rotation is summed for a given angle. Data are energy-corrected and linearity-corrected on-line on an event by event basis. Uniformity correction of each projection is done prior to tomographic reconstruction.

For brain studies, the cameras are set at the minimum radius of rotation (132 mm) and the headrest is attached to the base of the couch. The height of the headrest is fixed but the height of the couch can be adjusted for patient comfort. For the rest of the body, positioning is more time consuming in order to provide the best orbit, i.e., closest to the patient. During a continuous rotation acquisition, the radius of rotation of each camera remains fixed but during a step and shoot acquisition, the cameras can follow an elliptical path, ensuring closer patient proximity.

Received May 19, 1992; revision accepted Apr. 26, 1993.

For correspondence contact: Kypros Kouris, PhD, Institute of Nuclear Medicine, University College and Middlesex School of Medicine, Mortimer St., London W1N 8AA, UK.

Planar Measurements

Energy Resolution. Energy resolution measurements on the GCA-9300A were made using five different radionuclides: ^{57}Co (122 keV), ^{67}Ga (92 and 182 keV), ^{99m}Tc (140 keV), ^{123}I (159 keV) and ^{201}Tl (x-rays centered at 71 keV).

Planar Uniformity. The intrinsic planar uniformity was assessed for each camera in turn by removing the collimator and placing a ^{99m}Tc point source on the central axis of the camera at a distance of 2 m. The system's planar uniformity was assessed for each camera using a ^{57}Co flood source placed on the parallel-hole collimator.

Planar Sensitivity. For the parallel-hole collimators, the planar point source sensitivity was measured for each camera using a ^{99m}Tc point source of known activity placed in air 100 mm from the collimator. For the fanbeam collimators, measurements were only performed with the cameras set to their minimum radius of rotation (132 mm) and the source at the center of the FOV. The relative planar sensitivities of the three cameras over the entire FOV were evaluated by imaging the ^{57}Co flood on each camera in turn for the same amount of time for both collimator sets.

Planar System Spatial Resolution. The planar system spatial resolution in air was measured for the cameras fitted with the HR-PH collimators. A ^{99m}Tc point source was placed at the center of the FOV and static images (512^2 matrix) were acquired at 10, 50, 100, 132, 150, 200 and 250 mm from the collimator face. The variation of planar resolution with radial distance from the center of the FOV was examined using five-line sources in air parallel to the collimator face at 132 mm with the first in the center of the FOV and the others 20 mm apart.

Planar Collimator Response. A phantom consisting of 14 parallel-line sources (diameter < 2 mm) 30 mm apart on a thin perspex slab was used to investigate possible spatial distortion as a function of distance from the collimator. Planar images (256^2 matrix) of the phantom were acquired at 0, 50, 100, 150, 200 and 250 mm for both collimators, for each camera with the lines parallel to both the x-direction and the y-direction.

Tomographic Measurements

Reconstructed Pixel Size. The reconstructed pixel size was measured using four ^{99m}Tc line sources approximately 100 mm long, fixed to a block of expanded polystyrene forming a square of dimension 160 mm and placed perpendicular to the cameras in the center of the FOV. A 60-frame, 360-degree step and shoot acquisition (6 degrees per step) was performed using a 128^2 matrix with the HR-PH collimators and a 256^2 matrix with the SHR-FB collimators. The latter were converted to parallel geometry data (128^2 matrix, 6 degrees per step).

Center of Rotation. A ^{99m}Tc point source was placed approximately 80 mm horizontally from the center of rotation (COR) at a measured point along the axis of rotation (y-axis). Data were acquired for each of the three cameras at each of five y-coordinates using both collimator sets. In each case, a 60-frame, clockwise, step and shoot acquisition was performed over a 360-degree rotation (6 degrees per step) with the minimum radius of rotation (132 mm). The data for the parallel-hole collimators were acquired using a 128^2 matrix. For the fanbeam collimators, the data were collected using a 256^2 matrix and then converted to parallel geometry data with a matrix size of 128^2, 6 degrees per step. In addition, a single acquisition for each collimator was performed with the cameras rotating in a counterclockwise direction to determine if there was any mechanical hysteresis.

The COR analysis on the Toshiba computer required the point source to be placed at the center of the FOV which did not permit an adequate analysis of the system response. The data files were therefore transferred from the Toshiba computer to a DEC VAXstation via an IBM-compatible PC and were analyzed using a code written in VAX FORTRAN. For a given camera, collimator and y-coordinate of the point source, the following four graphs were plotted:

1. x-coordinate of the center of the source activity at each camera angle (obtained using a Gaussian fit). For a perfect system this should be a perfect sinusoid of a 360-degree period with amplitude equivalent to the maximum displacement of the source from the COR.
2. y-coordinate of the center of the source activity at each camera angle (obtained using a Gaussian fit). For a perfect system this should be a horizontal straight line, i.e., constant y-coordinate corresponding to the slice position.
3. Residual obtained by subtracting a fitted sinusoid of 360-degree period (first order Fourier analysis) from the measured x-coordinate. This shows the deviation of the x-coordinate from a perfect sinusoid and for a perfect system it should be a horizontal straight line at zero.
4. Average of the x-coordinate at camera angle ϕ and at ϕ + 180 degrees. For a perfect system this should be a horizontal straight line at the mean x-coordinate.

It is the mean of the x-coordinate data that is taken to represent the position of the COR and used by other manufacturers to calculate the COR-offset correction.

Inter-Camera Alignment. The projections from each acquisition for the COR experiments were merged to investigate whether a y-shift was present during rotation. The x-axis and y-axis alignment of the three cameras with respect to each other was also examined by performing tomographic acquisitions of a ^{99m}Tc point source in air and at the center of the FOV for each camera separately and all three together and then comparing the reconstructed coordinates of the source. Step and shoot acquisitions were performed with both collimator sets.

Stability of Planar Sensitivity with Angle. Using a ^{99m}Tc point source in air at the center of the FOV and at 132 mm radius of rotation, acquisitions were performed with each camera separately and all three together with both collimator sets using continuous and step modes. The effect of clockwise or counterclockwise rotation was also examined. The stability of sensitivity with angle was assessed by comparing the total counts in each of the planar projections. Acquisitions were also performed with a ^{57}Co point source taped on the face of each camera in turn to check whether there were any variations of sensitivity or rotational speed with angle; both continuous and step modes were employed.

Tomographic Volume Sensitivity. A cylinder (200 mm in diameter × 300 mm) containing an accurately measured amount of ^{99m}Tc uniformly mixed in water was placed in the center of the FOV parallel to the axis of rotation. Tomographic acquisitions were performed using the step and continuous rotation modes, at 6 degrees per step, and matrix size 64^2 for both parallel and fanbeam collimators noting the exact time each acquisition started and finished. A 20% energy window was used, placed symmetrically on the peak and shifted by 3% to the high-energy side. Using the total counts acquired within the central 102-mm length of the FOV, the actual time of data acquisition (i.e., 20 × time per step whether step or continuous mode) and the activity used (decay

corrected), the tomographic volume sensitivity was expressed as kcps/(MBq/ml)/cm.

Tomographic Uniformity. A cylinder (200 mm in diameter × 190 mm) containing approximately 700 MBq of ^{99m}Tc uniformly mixed in water was placed in the center of the FOV parallel to the axis of rotation. Tomographic acquisitions were performed using the step mode at 4 degrees per step, 30 M counts and matrix size 128^2 and 256^2 for the parallel and fanbeam collimators, respectively; the latter were converted to parallel geometry data at 128^2 and 4 degrees. Nonuniformities were evaluated in 12-mm thick reconstructed slices (4 pixels for HR-PH and 7 pixels for SHR-FB) using horizontal and vertical profiles.

Tomographic Spatial Resolution. The tomographic reconstructed spatial resolution was measured using ^{99m}Tc capillary line sources in air and in water using both collimator sets and a 20% symmetric energy window under a wide variety of acquisition conditions. All reconstructions were done using no prefilter, a ramp backprojection filter and no attenuation correction.

First, with a single point source at the center of the FOV, the reconstructed spatial resolution was measured for each camera separately and all three together using both collimator sets. Then, with three horizontal, parallel-line sources radially spaced at 0, 40 and 80 mm from the center of the FOV, several acquisitions were performed. For the parallel-hole collimators, different radii of rotation were used (132, 150, 200, 250 and 300 mm) with 4-degree steps and 128^2 matrix. At a radius of 132 mm, acquisitions using 3-degree and 6-degree steps were also performed. Both step and continuous (single) rotation modes were employed. For the fanbeam collimators, acquisitions were performed at 132 mm radius of rotation with 4-degree steps (256^2 matrix) converted to 4 degrees, (128^2 matrix), and with 6-degree steps, (256^2 matrix) converted to 6 degrees, (128^2 matrix). These acquisitions were also performed with both step and continuous (single) rotation modes.

The effect of employing the multiple-rotation mode on the tomographic spatial resolution in air was also examined. Eight rotations were used, the data from corresponding frames on each rotation were summed subsequently to acquire data for 2, 3, 7 and 8 rotations for the parallel-hole collimators at a 200-mm radius of rotation and for fanbeam collimators (132-mm radius of rotation). All acquisitions utilized 6-degree steps and 128^2 matrix. For the parallel-hole collimators, acquisitions were also performed at a radii of rotation of 132, 150, 250 and 300 mm but only the sum of all eight rotations was used.

To allow comparison with previously published values of reconstructed spatial resolution (*7,10*), two additional acquisitions were performed: parallel-hole collimators, step and shoot, 4 degrees per step (128^2 matrix), enlargement factor ×1.5 and radii of rotation of 132 and 200 mm; fanbeam collimators, 2 degrees per step, (256^2 matrix) converted to 4 degrees per step (128^2 matrix) parallel geometry data. The three-line sources and the Toshiba five-line source phantom were used. The latter comprises a line at the center and four lines at 75 mm from the center, 90 degrees apart. Central, radial and tangential FWHM values were calculated as the average from three slices, 10 mm thick and 40 mm apart.

In order to assess the effect of an asymmetric energy window on reconstructed spatial resolution and contrast, five horizontal ^{99m}Tc line sources in water (20 mm apart) were scanned at a 132-mm radius of rotation with both collimator sets using a 20% energy window both symmetric and asymmetric (3% offset).

Tomographic Linearity of Response. In order to assess the quantitative response of the system to different activity concentrations, five vials (35 mm diameter × 60 mm) were scanned and filled with water containing 10–100 MBq which varied from 10–100 MBq. The vials were supported horizontally on the back plate of a 200-mm diameter cylinder with one vial at the center and the others at a radius of 75 mm and 90 degrees apart. Acquisitions were performed with the vials in the air and the cylinder filled with water using both collimator sets. Reconstructions were done with no prefilter, and a ramp backprojection filter without attenuation correction as well as with attenuation correction. Regions of interest (ROIs) of 16 × 16 mm^2 were placed in the center of each vial to determine the relative activity concentrations in a central reconstructed slice thickness of about 12 mm (4 pixels for HR-PH and 7 pixels for SHR-FB).

Hoffman Three-Dimensional Brain Phantom Studies. The Hoffman three-dimensional brain phantom (*11*) was used to evaluate the effects of the various acquisition and processing parameters on reconstructed image quality and on reconstructed average grey matter-to-white matter ratio. This phantom mimics the three-dimensional normal anatomy of the human brain and reproduces the 4:1 ratio that is observed for normal grey and white matter blood flow. The phantom was carefully filled with uniformly mixed ^{99m}Tc in distilled water to which a small quantity of wetting agent was added to ensure that no significant air bubbles remained trapped. Acquisitions were performed with both collimator sets at the minimum radius of rotation. All HR-PH projections were 128^2 matrix; SHR-FB projections were 256^2 but converted to 128^2 matrix, parallel geometry data. Both continuous and step modes were employed for 60, 90 and 120 frames. The effects of filtering and converting from 2 degrees per step for fanbeam data to 3-, 4- and 6-degrees for parallel data were also investigated. To assess the effect of using an asymmetric energy window on reconstructed contrast resolution, the Hoffman three-dimensional brain phantom was scanned with both collimator sets at 132-mm radius of rotation using both symmetric and asymmetric (3% offset) energy windows.

RESULTS

Planar Measurements

Energy Resolution. The energy resolution was determined by obtaining a curve of the pulse-height spectrum and determining the FWHM of the peak(s) using linear interpolation. This was then expressed as a percentage of the peak energy. The energy was calibrated by means of a graph of energy versus a pulse-height analyzer channel corresponding to the peak of the pulse-height spectrum for the different nuclides investigated. The energy range covered by the calibration curve was 71–182 keV and was found to be linear ($r = 0.999$). The percentage FWHM energy resolution of the GCA-9300A for ^{99m}Tc was 10.1% (average value for all three cameras) compared with <10.6% (worst value) and 9.6% (typical value) as quoted in the GCA-9300A NEMA specification sheet.

Planar Uniformity. The planar extrinsic uniformity over the useful field-of-view (UFOV) was assessed using the HR-PH collimators, a ^{57}Co flood phantom and a 20% symmetric energy window (Table 1). The intrinsic nonuniformity parameters were very close to the extrinsic values indicating that the collimator contribution to nonuniformity was minimal except for camera B.

TABLE 1
Quantitative Assessment of the Planar Performance of the Toshiba GCA-9300A System

Extrinsic planar uniformity using HR-PH collimators		
Camera	Integral (%)	Differential (%)
A	3.6	2.1
B	4.1	2.5
C	3.5	1.8

Technetium-99m point source sensitivity in air (cps/MBq)		
Camera	HR-PH at 100 mm	SHR-FB at 132 mm
A	74.6	83.1
B	75.1	81.1
C	74.8	81.9

Planar spatial resolution as a function of distance from the HR-PH collimator of camera A		
Distance (mm)	FWHM (mm)	FWTM (mm)
10	4.4	7.9
50	6.0	10.5
100	8.0	13.9
132	9.3	16.5
150	10.1	17.7
200	12.4	21.4
250	14.4	25.5

Planar Sensitivity. The three cameras of the GCA-9300A have an almost equal point source sensitivity of 100%, 100.7% and 100.3% at 100 mm in air for the HR-PH collimators (Table 1). The point source sensitivity of the SHR-FB collimators varies with the distance from the collimator and was only measured with the source at the center of the FOV at 132 mm in air. Expressed as percentages, these sensitivity values were 100%, 97.5% and 98.5%, respectively. The relative planar sensitivities of the three cameras, obtained using a ^{57}Co flood phantom on each collimator were equal within 0.8% for the HR-PH and 2.7% for the SHR-FB collimators.

Planar System Spatial Resolution. The planar pixel size for the HR-PH collimators was measured as 0.80 mm using a 512^2 matrix in both the x- and y-directions. For the resolution, the FWHM was determined by linear interpolation. The variation of planar system spatial resolution with distance in air is given in for the HR-PH collimator of camera A. Corresponding values for the other cameras were within ±0.2 mm (Table 1). The spatial resolution was constant to within ±0.2 mm with radial distance from the center of the FOV at 132 mm from the face of the collimator.

Planar Collimator Response. Figure 1 presents qualitatively the planar collimator response at different distances from the collimator face. The parallel-hole collimators exhibited minimal (negligible) distortions. However, with the fanbeam collimators, significant nonlinearities were evident with increasing distance of the phantom from the collimator face.

Tomographic Measurements

Reconstructed Pixel Size. The reconstructed pixel size for 128^2 matrix obtained using four-line sources arranged in a square of size 160 mm perpendicular to the axis of rotation was 3.2 mm and 1.735 mm for the HR-PH and SHR-FB collimators, respectively. In spite of the nonlinear distortions observed in planar images with the SHR-FB collimators (Fig. 1), there were no distortions in transaxial slices as shown in Figure 2.

Center of Rotation. Representative results from the COR experiments performed with a ^{99m}Tc point source at five different y-positions for each camera for both collimator sets are presented in Figure 3. The parallel-hole collimators exhibited a better response than the fanbeam collimators. The slight sinusoidal trend seen on the graphs of y-coordinate versus camera angle suggests a slight camera tilt away from the horizontal axis of rotation; the maximum deviation was about ±0.8 mm for the parallel-hole collimators compared to ±1.7 mm for the fanbeam collimators. The spread in the x-residual was about ±0.6 mm for the parallel-hole collimators compared to ±2.6 mm for the fanbeam collimators. Irrespective of the y-position of the point source, fanbeam collimator problems were primarily evident for gantry angles 0–120° for all cameras suggesting a regional defect in the collimator manufacturing mold (since at these positions the point source would have been imaged in the same region of the collimator).

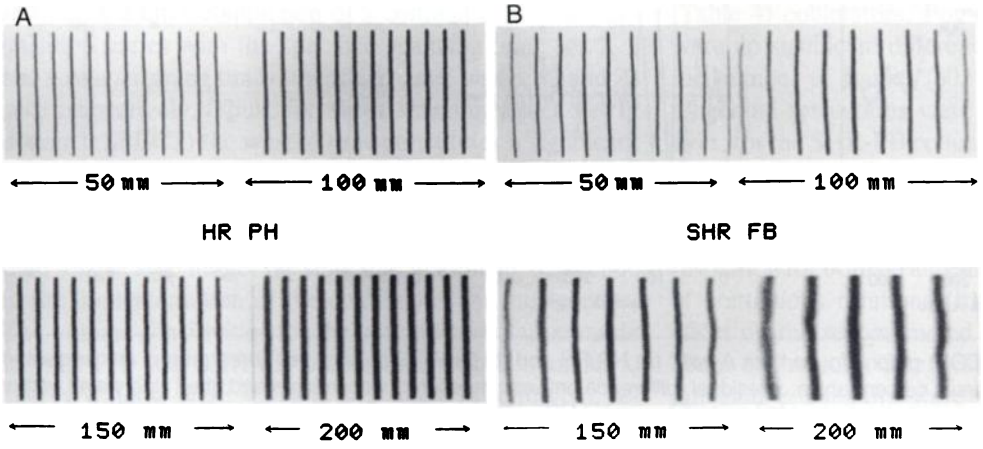

FIGURE 1. Planar collimator response to a phantom comprising parallel line sources placed parallel to the collimator face (camera A) at 50, 100, 150 and 200 mm in air from the HR-PH (A) collimator and the SHR-FB collimator (B). Nonlinear distortions are evident with increasing distance from the SHR-FB collimator.

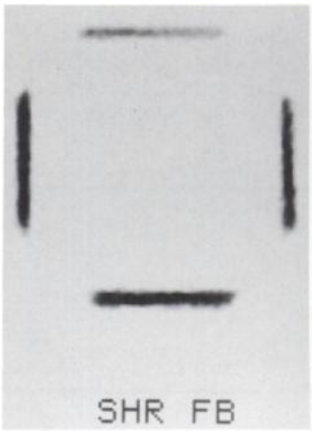

FIGURE 2. Transaxial slice through four-line sources in a square arrangement perpendicular to the axis of rotation in the center of the FOV with the SHR-FB collimators. No distortions are evident.

Inter-Camera Alignment. There was no visually apparent y-shift in the merged point source projections (of the COR experiments) from each camera. The average of the five mean x-coordinates (COR) for the five y-positions were 63.65, 63.61 and 63.46 pixels for cameras A, B and C, respectively, for the HR-PH collimators, and 63.56, 63.69 and 63.24 pixels for the SHR-FB collimators. Thus, the maximum difference between cameras was 0.6 and 0.8 mm for the parallel-hole and fanbeam collimators, respectively. The x- and y-coordinates (in pixels, 128^2 matrix) were 65 and 64 for a ^{99m}Tc point source at the center of the FOV reconstructed separately with each camera and all three cameras together, for both parallel-hole and fanbeam collimators, indicating that there was no detectable misalignment.

Stability of Planar Sensitivity with Angle. The planar sensitivity of each camera to a ^{99m}Tc point source at the center of the FOV in air was constant within 5.6% maximum deviation for the HR-PH collimators and 7.9% for the SHR-FB collimators. The percent integrated counts over

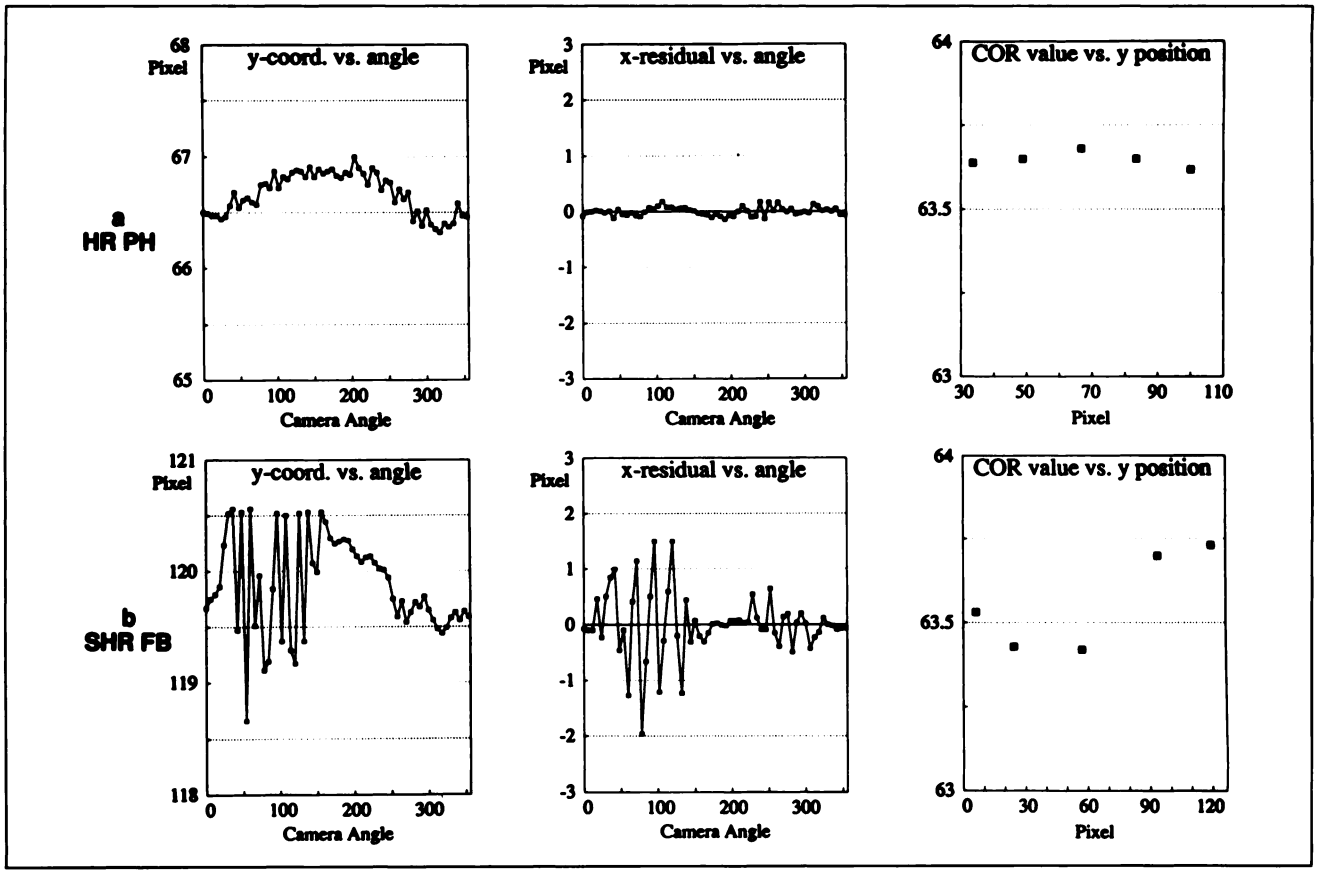

FIGURE 3. Center of rotation (COR) graphs for camera A with: (a) HR-PH and (b) SHR-FB collimators. Three graphs are presented: y-coordinate of the point source versus camera angle; x-residual (difference between measured x-coordinate and fitted sine wave) versus camera angle; and COR value (expressed in pixels, 128^2 matrix) for each of five y-coordinates of a point source placed 80 mm from the center of the FOV.

TABLE 2
Tomographic Volume Sensitivity (kcps/(MBq/ml)/cm) Using a 20% Energy Window Over Actual Time of Data Acquisition

Collimator	% offset	Volume sensitivity		
		Step	Continuous	Mean
HR-PH	0%	32.5	33.8	33.2
	3%	29.4	30.5	30.0
SHR-FB	0%	33.3	34.8	34.1
	3%	30.4	31.5	30.9

all projections for each camera separately and all three together were 100%, 100.3%, 100.1% and 99.4%, respectively, with the HR-PH collimators and 100%, 97.4%, 97.2% and 99.8%, respectively, with the SHR-FB collimators. There was no significant difference with direction of rotation or acquisition mode (continuous or step). Similarly, with the ^{57}Co point source taped on the collimator face, the number of counts per projection was independent of the angle and no differences were observed between continuous or step acquisitions. The percent integrated counts over all projections for each camera were 100%, 101.5% and 101.8%, respectively, for the step mode and 100%, 101.4% and 101.7%, respectively, for the continuous rotation mode.

Tomographic Volume Sensitivity. The tomographic volume sensitivities of the GCA-9300A with HR-PH and SHR-FB collimators are given in Table 2 using both symmetric and asymmetric (3% offset) 20% energy windows for both step and continuous rotation modes. The two collimators have almost equal volume sensitivity. The quoted volume sensitivities represent the maximum values since they were calculated using the time period of actual data acquisition, i.e., excluding the time during which the gantry rotates from one step to the next in the step and shoot acquisition mode or the time prior to starting and after completion of the 120-degree rotation in the continuous rotation mode. The gantry rotation time for step and shoot acquisition varies between 8–12 sec for different angular step size and acquisition time. The time prior to starting and after completion of a continuous rotation acquisition varies with the specified scanning time: for 1, 2 and 5 min scanning times, the 'dead time' was 8, 13 and 22 sec, respectively. Thus, for short scanning times (as in dynamic SPECT) the wasted time constitutes a significant fraction of the total imaging time and, consequently, the effective tomographic volume sensitivity is reduced. The volume sensitivity for continuous rotation was 4.0% higher than for the step mode; possibly due to a timing difference in the implementation of the continuous and step modes. The volume sensitivities for the continuous rotation mode for HR-PH and SHR-FB collimators with a symmetric energy window were 33.8 and 34.8 kcps/(MBq/ml)/cm, respectively. The drop in volume sensitivity by using a 3% offset was 9.6% and 9.2% for the HR-PH and SHR-FB collimators, respectively. With a symmetric 15% energy window, the drop in sensitivity was 10.8% and 11.2%, respectively.

Tomographic Uniformity. Tomographic uniformity was assessed in 12-mm thick slices reconstructed without prefiltering and with the ramp backprojection filter. With parallel-hole collimators, attenuation correction resulted in a more uniform image (i.e., smaller fractional s.d. as described by horizontal and vertical profiles). With the fanbeam collimators, the reconstructed distribution was more uniform without attenuation correction. This is in agreement with a Toshiba recommendation not to apply attenuation correction for fanbeam brain SPECT. (Attenuation correction was performed using Toshiba software with an attenuation coefficient of 0.12. An interactive threshholding method was used to determine body outline. Horizontal and vertical profiles of 12-mm thick strips through the center of the FOV gave ±15% (s.d./mean) for the HR-PH collimators and ±11% for SHR-FB collimators.

Tomographic Spatial Resolution. Measurements with ^{99m}Tc line sources in air and water for both collimator sets under a variety of acquisition conditions are presented in Tables 3–6.

There were no differences (< ±0.1 mm) in the FWHM or FWTM tomographic spatial resolution obtained with a ^{99m}Tc point source in air scanned with each camera separately and all three cameras together fitted with either HR-PH or SHR-FB collimators. With the cameras set at the minimum radius of rotation (132 mm) and using 90 frames, the tomographic spatial resolution in air at the center of the FOV was 10.2 and 7.8 mm FWHM with the HR-PH and SHR-FB collimators, respectively (19.0 and 13.8 mm FWTM). These values are in agreement with those of Ichihara et al. (*10*): 10.0 and 7.5 mm, respectively. Slightly better values (9.8 mm FWHM, 17.6 mm FWTM) were obtained for the HR-PH collimators by using a 1.5× enlargement factor (Table 3), because of the improved spatial sampling. The direction of gantry rotation had no effect (< ±0.1 mm) on the measured reconstructed spatial resolution. There were no significant differences in the FWHM or FWTM values between continuous or step acquisition modes for either parallel (Table 3) or fanbeam (Table 4) collimators. For the HR-PH collimators, there were no significant differences in FWHM or FWTM with the number of frames (60, 90 or 120) and the radial and tangential resolutions were about equal (Table 3). However, for the SHR-FB collimators, the tangential resolution at 80 mm from the center with 60 frames was significantly inferior (by about 2 mm FWHM) compared to that with 90 frames; the tangential resolution was worse than the radial resolution for both 60 and 90 frames (Table 4). The number of continuous rotations (from 2 to 8) had no significant effect on the reconstructed resolution for parallel or fanbeam collimators. The best estimates of resolution with fanbeam collimators were obtained with 2-degree steps (256^2 matrix) converted to 4 degrees, (128^2 matrix) (Table 4). But even at this improved angular sampling, the tangential resolution is worse than the radial. The central,

TABLE 3
Tomographic Spatial Resolution in Air Using the HR-PH Collimators

Variation of tomographic spatial resolution in air with different number of frames (60, 90 and 120) using HR-PH collimators, 132-mm radius with both continuous and step modes

Description	Radial distance (mm)	Radial (mm)		Tangential (mm)	
		FWHM	FWTM	FWHM	FWTM
Continuous (60 frames)	0	10.9	19.3	10.8	19.6
	40	10.8	19.3	10.8	20.1
	80	10.3	18.7	11.8	22.9
Continuous (90 frames)	0	10.2	19.0	10.5	19.4
	40	10.6	19.0	10.9	19.6
	80	11.3	19.8	10.6	20.4
Continuous (120 frames)	0	10.8	19.4	10.8	19.6
	40	10.8	19.3	10.5	19.4
	80	10.4	18.7	10.9	20.9
Step (60 frames)	0	10.8	19.2	10.7	19.8
	40	10.9	19.3	10.6	19.8
	80	10.4	18.7	10.4	20.2
Step (90 frames)	0	10.3	18.6	11.0	19.7
	40	10.3	18.5	10.9	20.3
	80	11.1	19.8	9.9	20.9
Step (120 frames)	0	10.8	19.3	11.4	19.8
	40	10.8	19.2	10.4	19.6
	80	10.3	18.6	10.3	19.8

Tomographic spatial resolution of HR-PH collimators at a 132-mm and 200-mm radius of rotation using step, 90 frames, and enlargement ×1.5

Radius of rotation (mm)	Radial distance (mm)	Radial (mm)		Tangential (mm)	
		FWHM	FWTM	FWHM	FWTM
132	0	9.8	17.6	9.6	17.5
	40	9.9	17.4	9.5	17.5
	80	10.0	17.8	8.1	17.4
200	0	12.8	22.2	12.9	22.2
	40	12.8	22.6	12.1	21.7
	80	12.8	22.3	10.8	21.8

radial and tangential FWHM values obtained using the Toshiba five-line source phantom are presented in Table 5. During a 6-mo period, the reproducibility of these measurements was ±0.1 mm.

In water, the tomographic spatial resolution at the center of the FOV and 132 mm radius of rotation was 11.0 and 7.8 mm FWHM with the HR-PH and SHR-FB collimators, respectively (20.6 and 14.5 mm FWTM) (Table 6). The degradation of tomographic spatial resolution with increasing radius of rotation is presented in Table 6 for the HR-PH collimators.

With a 20% symmetric energy window, the average peak-to-valley ratio of five-line sources spaced by 20 mm in water (five peaks and four valleys) was 4.6 and 11.1 for the parallel-hole and fanbeam collimators, respectively. The difference is due to the different pixel sizes (3.2 mm for HR-PH and 1.735 mm for SHR-FB) and the superior spatial resolution of the SHR-FB collimators. With a 3% offset, the average peak-to-valley ratio improved by only 2.8% for the parallel-hole collimators but there was a 13.7% improvement for the fanbeam collimators. There was no improvement in FWHM spatial resolution with the asymmetric energy window.

Tomographic Linearity of Response. The quantitative response of the system to the same activity concentration in different areas of the FOV is presented in Table 7. Scans were performed with both collimator sets, with the vials in the air as well as in a water-filled cylinder. Each set of estimated concentrations was normalized with respect to the average of the five reconstructed values. With the vials in water, the activity in the central vial is severely underestimated if attenuation correction is not used.

Similarly, the quantitative response of the system to different relative activity concentrations (expressed in the range 0.0–1.0) was evaluated using vials containing accurately measured quantities of ^{99m}Tc. Reconstructions were performed with and without attenuation correction (linear attenuation coefficient 0.12 cm^{-1}). In each experiment, the central vial contained the highest activity and was used for normalizing the other four estimated concentrations. Estimated relative activity concentrations were similar for the two collimator sets, and they were more accurate in water if attenuation correction was used. Values without attenuation correction were overestimated for both collimator sets because the central vial (with respect to which normalization was performed) was underestimated. Figure 4

TABLE 4
Tomographic Spatial Resolution in Air Using the SHR-FB Collimators

Tomographic spatial resolution in air with SHR-FB collimators using step 256^2, 2 degrees per step converted to 128^2, 4 degrees per step

Radial distance (mm)	Radial (mm)		Tangential (mm)	
	FWHM	FWTM	FWHM	FWTM
0	7.8	13.8	8.5	14.1
40	8.0	14.4	8.5	15.2
80	8.3	14.8	8.6	15.3

Variation of tomographic spatial resolution in air with step and continuous modes, and number of frames (60 and 90) with the SHR-FB collimators ($256^2 \rightarrow 128^2$)

Description	Radial distance (mm)	Radial (mm)		Tangential (mm)	
		FWHM	FWTM	FWHM	FWTM
Step (90 frames; 4° → 4°)	0	7.9	13.8	8.3	14.8
	40	8.3	14.4	8.9	15.3
	80	8.1	14.8	9.6	17.3
Continuous (90 frames; 4° → 4°)	0	7.9	13.8	8.5	14.9
	40	8.3	14.4	9.0	15.6
	80	8.4	14.9	10.1	18.0
Step (60 frames; 6° → 6°)	0	7.9	13.9	8.0	15.2
	40	8.3	14.4	9.4	16.0
	80	8.4	15.2	11.6	19.9
Continuous (60 frames; 6° → 6°)	0	8.0	14.1	8.5	14.8
	40	8.4	14.5	10.0	17.1
	80	8.5	15.2	12.8	23.1

shows that there is an excellent linear relationship between true and estimated relative activity concentrations and if attenuation correction is used, the relationship is close to the identity line (for the HR-PH collimators: slope = 1.02, intercept = 0.03, r = 0.997; for the SHR-FB collimators: slope = 0.98, intercept = 0.04, r = 0.997).

Hoffman Three-Dimensional Brain Phantom. Figure 5 demonstrates the excellent image quality achieved by the Toshiba GCA-9300A in imaging the Hoffman three-dimensional brain phantom using both collimator sets with 132-mm radius of rotation. In both cases, the total number of counts in the 'brain' (i.e., excluding the uniform part of the phantom) was about 40 M counts; reconstruction was performed using the Butterworth prefilter with power 8 and the ramp backprojection filter with attenuation correction for the parallel-hole collimator and without attenuation correction for the fanbeam collimator. A linear grey scale and standard Toshiba threshholding of 10%–105% was used to display the images. Image quality with the SHR-FB collimators is superior.

For quantitative analysis, the same transaxial slice through the thalami and basal ganglia of the Hoffman three-dimensional brain phantom was reconstructed for a variety

TABLE 5
Tomographic Spatial Resolution (FWHM mm) Obtained Using the Toshiba Five-Line Source Phantom Filled with ^{99m}Tc with HR-PH (radii of rotation 132 and 200 mm) and SHR-FB Collimators (132-mm radius)

FWHM (mm)	HR-PH 132 mm	HR-PH 200 mm	SHR-FB 132 mm
Central	10.6	13.1	7.6
Radial	10.2	13.1	8.1
Tangential	9.1	11.6	7.0

TABLE 6
Tomographic Spatial Resolution in Water With HR-PH and SHR-FB Collimators

Variation of tomographic spatial resolution in water at different radii of rotation using the HR-PH collimators, 90 frames, step

Radius (mm)	FWHM (mm)	FWTM (mm)
132	11.0	20.6
150	11.3	20.8
200	12.4	23.3
250	14.2	26.4
300	16.8	31.3

Variation of tomographic spatial resolution in water using the SHR-FB collimators

Description	Radial distance (mm)	Radial (mm)		Tangential (mm)	
		FWHM	FWTM	FWHM	FWTM
60 frames	0	7.8	14.3	7.9	15.0
	40	8.5	17.0	8.0	15.8
	80	9.8	18.8	12.2	21.4
90 frames	0	7.8	14.5	7.8	14.8
	40	8.3	16.8	7.2	16.2
	80	9.4	18.2	9.3	15.8

TABLE 7
Tomographic Response to the Same Activity Concentrations in Different Areas in the FOV in Air and in a Water-Filled Cylinder

Vials	Measured	Estimated in air		Estimated in water (no attenuation correction)		Estimated in water (with attenuation correction)	
		HR-PH	SHR-FB	HR-PH	SHR-FB	HR-PH	SHR-FB
A	1.0	0.85	0.86	0.75	0.75	0.93	0.95
B	1.0	1.00	1.00	1.03	1.04	1.03	1.05
C	1.0	1.00	1.00	0.99	0.98	0.99	1.00
D	1.0	0.98	0.99	0.98	0.98	0.97	0.95
E	1.0	1.02	1.00	0.99	0.99	1.00	1.00

of different acquisitions and/or processing conditions. The slice thickness was commonly 6.4 mm for the HR-PH collimators (i.e., 2 pixels thick) and 7.0 mm for SHR-FB (i.e., 4 pixels thick); however, quantitatively, there was no significant difference if half the slice thickness was used. The average grey matter-to-white matter ratios obtained using square ROIs in the same positions for each different set of conditions are listed in Table 8. Eighteen ROIs were used for the grey matter and seven for the white matter. The size of the ROI was 8.7 × 8.7 mm^2, corresponding to about 1× the FWHM spatial resolution. All values are significantly less than 4:1, the theoretical value, due to the partial volume effect. There was no quantitative difference in grey matter-to-white matter ratio between step or continuous acquisition modes, for either parallel or fanbeam collimators. Adding projection data from more than one rotation causes a reduction in the grey matter-to-white matter ratio (Table 8). The effect of angular sampling and fanbeam to parallel rebinning is presented in Table 8. In the presence of high counts (and hence low noise), a higher cut-off frequency filter yields a higher grey matter-to-white matter ratio; even so, the maximum value obtained using a symmetric window was only about 2.3 with the Butterworth filter, power 8 and a cut-off frequency of 0.8 cycles/cm. Use of an asymmetric energy window (3% offset) gave no improvement in grey matter-to-white matter ratio for the parallel-hole collimators and only a 5.6% improvement for fanbeam collimators (from 2.30 to 2.43, Table 8). There was a slight visual improvement in image quality with the asymmetric window using the SHR-FB collimators.

In routine clinical brain studies using SHR-FB collimators, the total counts acquired are typically about 4–5 M counts and the average grey matter-to-white matter ratio is only about 1.7 (using the Butterworth prefilter with power 8 with 0.6 cycles/cm critical frequency and no attenuation correction). A similar value (1.73) was obtained with a 4.0-

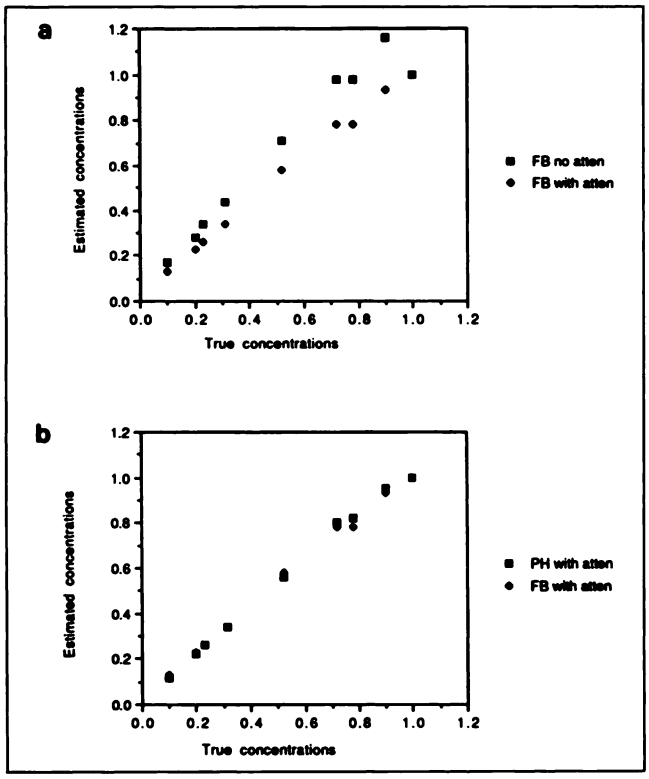

FIGURE 4. Quantitative response of the Toshiba GCA-9300A system to different relative activity concentrations: (a) Using SHR-FB collimators with and without attenuation correction and (b) using HR-PH and SHR-FB collimators with attenuation correction.

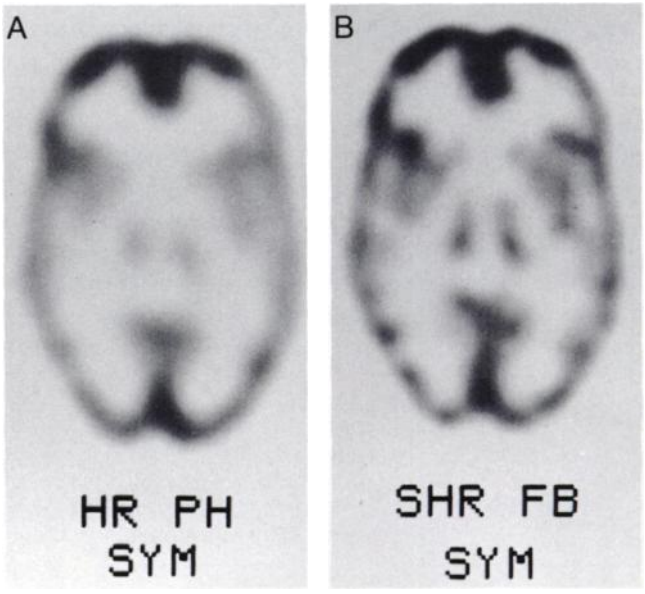

FIGURE 5. Image quality achieved by the Toshiba GCA-9300A in imaging the Hoffman three-dimensional brain phantom with 132-mm radius of rotation and 20% symmetric energy window using the HR-PH collimators and SHR-FB collimators with similar acquisition, processing and display conditions.

TABLE 8
Variation of Reconstructed Grey-to-White Matter Ratio with Different Acquisition and Processing Parameters Using the Hoffman Three-Dimensional Brain Phantom, 40 M counts

HR-PH, effect of number of continuous rotations	
Description	Ratio
1 rotation; 6° 128	2.28
2 rotations; 6° 128	2.22
3 rotations; 6° 128	2.18
7 rotations; 6° 128	1.99
8 rotations; 6° 128	1.98
SHR-FB, effect of angular sampling and fanbeam to parallel rebinning, $256^2 \rightarrow 128^2$	
Description	Ratio
Step; 2° → 3°	2.27
Step; 2° → 4°	2.23
Step; 2° → 6°	2.33
Step; 4° → 4°	2.10
Step; 4° → 6°	2.09
Cont.; 4° → 6°	2.10
Step; 6° → 6°	2.10

Effect of symmetric versus asymmetric energy window	Ratio	
Collimator	Symmetric	Asymmetric
HR-PH	2.21	2.22
SHR-FB	2.30	2.43

M counts acquisition using the Hoffman three-dimensional brain phantom.

DISCUSSION

Collimator choice is one of the most important factors that determine image quality in nuclear medicine. In agreement with others (*12,13*), we recommend the use of high-resolution collimators in SPECT. Fanbeam collimators can further improve both resolution and sensitivity (*7,8,10,14*); the apparent system planar resolution improves by the magnification effect. Cone-beam collimation gives the highest sensitivity but requires a scanning trajectory that will yield sufficient angular sampling (*15,16*).

Multiheaded SPECT systems primarily offer a substantial increase in tomographic volume sensitivity compared to a single rotating gamma camera. Depending on collimator type and collimator design parameters, better tomographic spatial resolution is achievable. The Toshiba GCA-9300A triple-headed system achieves both objectives but suffers from its extremely slow computer. With the equipment and collimators available at our institution, a comparison of measured tomographic sensitivity and spatial resolution in air is given in Table 9 for the Toshiba GCA-9300A, the GE/CGR Neurocam (*9*) and the GE 400XCT single rotating gamma camera. With the tungsten ultra high resolution (UHR) fanbeam collimators, the tomographic sensitivity and spatial resolution of the GCA-9300A are 17.0 kcps/(MBq/m)/cm and 5.9 mm FWHM, respectively

TABLE 9
Comparison of Tomographic Performance of Toshiba GCA-9300A, GE/CGR Neurocam and GE 400XCT Camera Using a 20% Symmetric Energy Window

Collimator	Toshiba GCA-9300A	GE/CGR Neurocam	GE 400XCT
Tomographic volume sensitivity (kcps/(MBq/ml)/cm)			
GP		50.7	12.8
HR	33.8	30.0	7.6
SHR-FB	34.8		
Tomographic spatial resolution in air (FWHM mm)			
GP		10.7	11.7
HR	10.2	9.0	10.3
SHR-FB	7.8		

GP = general purpose; HR = high resolution; and SHR-FB = super-high resolution fanbeam.

(*7,10*). The four-headed Osaka/Hitachi (Hitachi, Tiba, Japan) SPECT (*17*), a brain-dedicated system, utilizes four compact gamma cameras defining a square aperture of constant size and similar FOV; its sensitivity with high-resolution collimators is 22.2 kcps/(MBq/ml)/cm. The ASPECT (Digital, Waltham, MA) (*18*), another brain-dedicated system consisting of a stationary annular NaI(Tl) crystal and a rotating collimator system, gives 8.2 mm FWHM in air and a tomographic sensitivity of 27.0 kcps/(MBq/m)/cm.

We recognize that fanbeam collimators are difficult to manufacture but improvements in the manufacturing process would appear to be necessary for the Toshiba SHR-FB collimators because significant distortions were observed in planar images. Although there were no obvious artifacts in reconstructed images, we assume that there must be some underlying artifacts since reconstructed images can only be as good as the planar projections from which they originate.

Quality assurance (QA) of SPECT instrumentation aims to ensure optimum image quality (*19*). Compared to a single rotating gamma camera, the requirements of a triple-headed system are greater: each camera must be calibrated in turn (PMT tuning, linearity, energy and uniformity corrections) and tested separately with respect to planar sensitivity, resolution and uniformity for each collimator; head misalignment with respect to the center of rotation due to linear shifts must be corrected in both the x- and the y-(patient axis) directions, and there must be no angular misalignment between the three cameras. Having performed extensive planar and tomographic performance and QA tests over a 6-mo period, we have concluded that the Toshiba GCA-9300A is a well-calibrated and stable system. All calibrations are either done at the factory or on-site by the Toshiba engineers. This is a different philosophy to that of most other manufacturers where corrections for COR, energy and perhaps linearity are user calibrations. However, with either philosophy, the user must be able to test the system regularly in order to detect a malfunction before

TABLE 10
Comparison of Acquisition Protocols for ^{99m}Tc-HMPAO Brain Perfusion Studies Using the GE 400XCT Gamma Camera, the GE/CGR Neurocam and the Toshiba GCA-9300A

	GE 400XCT	GE/CGR Neurocam		Toshiba GCA-9300A
Collimators	HR	HR	GP	SHR-FB
No. of views	64	128	128	90 → 60
Energy window (offset %)	20% (3%)	20% (3%)	20% (3%)	20% (0%)
Matrix size	128	64	64	256 → 128
Pixel size (mm)	3.2	4.0	4.0	1.735
Time per view(s)	30–40	20	15	30
Total time (min)	35–45	15	11	15
Counts per view (kcnts)	50	35	50	55
Total counts (M counts)	3.2	4.5	6.4	5.1

it affects clinical scans. For example, it has been recommended that COR corrections should be checked every month and hence most manufacturers of SPECT equipment provide software which can be used to perform the required analysis. However, the COR corrections for the Toshiba GCA-9300A system are set at the factory and cannot be changed. Toshiba argues that a single COR correction factor for all angles and all projections is insufficient and that many correction factors should be used; acquiring the required data on-site is not considered feasible. The COR analysis code written for this work can be obtained from the authors.

For the parallel-hole collimators there was no significant improvement in either peak-to-valley or grey matter-to-white matter ratios with the use of an asymmetric energy window. However, for the fanbeam collimators, there was a significant quantitative improvement in the peak-to-valley ratio (13.7%) and a 5.6% improvement in the grey matter-to-white matter ratio. Moreover, with the fanbeam collimators, there was a qualitative improvement in image quality. Therefore, the routine use of either a 20% asymmetric energy window or a narrower symmetric energy window would be worth considering. Using a ^{57}Co flood, the loss of counts by using a 20% asymmetric window with 3% offset or a 15% symmetric energy window compared to 20% is about 10% and 11%, respectively, for the same imaging time.

Toshiba recommends that for brain studies utilizing the SHR-FB collimators, attenuation correction should not be used due to a depth compensation effect in the fanbeam to parallel conversion. We have found that the quantitative response of the system to different activity concentrations is only linear and close to the identity line if attenuation correction is used. Conversely, the tomographic uniformity of the system when using the SHR-FB collimators is degraded by the use of attenuation correction. We therefore conclude that the depth compensation effect is only valid for an extended source. As the brain approximates more closely to an extended source than to a series of discrete sources, the Toshiba recommendation not to use attenuation correction would seem to be appropriate.

In spite of the improved tomographic spatial resolution of the GCA-9300A with the SHR-FB collimators compared to the GE/CGR Neurocam with HR-PH collimators, the reconstructed grey matter-to-white matter ratios with the Hoffman three-dimensional brain phantom were lower (2.43 versus 2.60 under similar acquisition conditions and with the same filters). This may be due to differences in the reconstruction algorithm.

The SHR-FB collimators are used for brain studies and the HR-PH collimators for all other studies. Typical SPECT acquisition protocols used at our institution for brain perfusion studies with ^{99m}Tc-HMPAO are compared for a single rotating gamma camera, the GE/CGR Neurocam and the Toshiba GCA-9300A in Table 10. Typical values of resulting total counts if 740 MBq of ^{99m}Tc-HMPAO were administered and total acquisition times are also listed.

In conclusion, our measurements have confirmed that the Toshiba GCA-9300A triple-headed SPECT system achieves excellent image quality for both brain and body tomography. The most serious limitation is the computer but we understand that a new high-speed processor will soon be introduced. The gantry and detectors are well-designed, stable, reliable and sufficiently provide for patient safety. The introduction of planar static, dynamic and multigated capabilities from more than one camera would render the GCA-9300A a more general purpose system. The speed of rotation between steps should be increased thereby decreasing the 'dead-time' during scanning. Medium-energy collimators (and perhaps high-energy collimators) would be useful. A larger FOV would accommodate the lungs and it would be useful if the patient couch could move for a second scan of an adjacent body area.

ACKNOWLEDGMENTS

The authors wish to thank Professor P. J. Ell and Dr. D. C. Costa for their support and comments in the preparation of this manuscript; all the staff at the Institute of Nuclear Medicine, UCMSM, for their cooperation; Mr. T. Ichihara for his helpful technical discussions; and Toshiba Medical Systems for their co-operation.

REFERENCES

1. George MS, Ring HA, Costa DC, Ell PJ, Kouris K, Jarritt PH. *Neuroactivation and neuroimaging with SPET*. New York: Springer; 1991.
2. Hisada K, ed. *An atlas of second-generation SPECT*. Japan:Maruzen Planning Network Co.; 1991.
3. Blokland JAK, Reiber JHC, Pauwels EKJ. Quantitative analysis in single photon emission tomography (SPET). *Eur J Nucl Med* 1992;19:47–61.
4. Fahey FH. Dedicated cameras for SPECT. *SNM computer and instrumentation council newsletter* 1992;9:16.
5. Kouris K, Costa DC, Jarritt PH, Townsend CE, Ell PJ. Brain SPECT using a dedicated three-headed camera system. *J Nucl Med Technol* 1992;20:68–72.
6. Lim CB, Walker R, Pinkstaff C, et al. Triangular SPECT system for 3-D total organ volume imaging: performance results and dynamic imaging capability. *IEEE Trans Nucl Sci* 1986;33:501–504.
7. Ichihara T. Development of a high resolution SPECT system. *Toshiba Med Rev* 1990;33:29–35.
8. Moore SC, Kouris K, Cullum I. Collimator design for single photon emission tomography. *Eur J Nucl Med* 1992;19:138–150.
9. Kouris K, Jarritt PH, Costa DC, Ell PJ. Physical assessment of the GE/CGR Neurocam and comparison with a single rotating gamma camera. *Eur J Nucl Med* 1992;19:236–242.
10. Ichihara T, Matsudaira M, Yamada M. Basic development of the Toshiba digital gammacamera, model GCA-9300A. In: Hisada K, ed. *An atlas of second-generation SPECT*. Japan: Maruzen Planning Network Co.; 1991: 16.
11. Hoffman EJ, Cutler PD, Digby WM, Mazziota JC. Three-dimensional phantom to simulate cerebral blood flow and metabolic images for PET. *IEEE Trans Nucl Sci* 1990;37:616–620.
12. Muehllehner G. Effect of resolution improvement on required count density in ECT imaging: a computer simulation. *Phys Med Biol* 1985;30:163–173.
13. Mueller SP, Polak JF, Kijewski MF, Holman BL. Collimator selection for SPECT brain imaging: the advantage of high resolution. *J Nucl Med* 1986; 27:1729–1738.
14. Jaszczak RJ, Chang LT, Murphy PH. Single photon emission computed tomography using multi-slice fan beam collimators. *IEEE Trans Nucl Sci* 1979;26:610–618.
15. Gullberg GT. Convergent beam tomographic systems. *SNM computer and instrumentation council newsletter* 1991;9:2–6.
16. Gullberg GT, Zeng GL, Christian PE, Datz FL, Morgan HT. Cone beam tomography of the heart using SPECT. *Invest Radiol* 1991;26:681–688.
17. Kimura K, Hashikawa K, Etani H, et al. A new apparatus for brain imaging: a four-head rotating gamma camera single-photon emission computed tomograph. *J Nucl Med* 1990;31:603–609.
18. Genna S, Smith AP. The development of ASPECT, an annular single crystal brain camera for high efficiency SPECT. *IEEE Trans Nucl Sci* 1988;NS-35: 654–658.
19. AAPM Report No. 22. *Rotating scintillation camera SPECT acceptance testing and quality control*. New York: American Association of Physicists in Medicine; 1987.

EDITORIAL

Doing Well Under Pressure: Dedicated SPECT Cameras Come of Age

A diamond is a lump of coal that did well under pressure.

Anonymous

Over the past decade, SPECT has been practiced as an accessory to regular imaging. Cameras have been designed primarily for planar imaging with SPECT capabilities often added as an afterthought. Cost, unstable technology and reimbursement problems appeared to conspire to make SPECT imaging an unprofitable, although scientifically and clinically rewarding, endeavor. Recently, the picture has changed. Systems optimized for SPECT imaging or, in some cases designed exclusively for SPECT imaging, have become widespread and have been profitable for their vendors. More than 100 dedicated SPECT systems have been sold during the past twelve months in the United States alone.

Received and accepted July 5, 1993.

For correspondence and reprints contact: Jack E. Juni, MD, Nuclear Medicine Department, William Beaumont Hospital, 3601 West 13 Mile Road, Royal Oak, MI 48073-6769.

WHY NOW?

The advance of dedicated SPECT systems is due to the convergence of developments in technology assessment, camera construction, tracer development, collimation, computing and reimbursement practices.

Growth in nuclear cardiac imaging over the past decade has been enormous. Although SPECT has been developing for years, only recently has hard data appeared attesting to its superior clinical results. Fintel et al. (*1*) have shown that thallium SPECT imaging is superior to planar imaging. The development of ^{99m}Tc-sestamibi and ^{99m}Tc-teboroxime and effective ^{99m}Tc-labeled heart tracers has advanced the use of SPECT. To take advantage of the higher photon flux offered by these tracers, the interfering effects of adjacent liver and bowel activity that would otherwise obscure the inferior wall must be eliminated. Planar imaging of these tracers is clearly inferior to SPECT (*2,3*). The emergence of ^{123}I-iodoamphetamine, ^{99m}Tc-HMPAO and ^{99m}Tc-ethyl-cysteinate dimer for brain imaging has opened a vast new territory to the clinical practice of nuclear medicine (*4*). These tracers are only of value when imaged tomographically. The detailed structure of the brain demands the highest imaging quality possible and, in many centers, has driven the move to dedicated SPECT imagers.

Perhaps the most important development in dedicated SPECT cameras has been the reintroduction of multidetector systems. Dual-headed, SPECT-capable gamma cameras were available over a decade ago but were not particularly successful. Although many aspects of SPECT imaging technology have improved since that time, the primary obstacle with these units was difficulty in aligning the two detectors. In an attempt to provide maximum flexibility, camera designers furnished multiple independent axes of motion for each detector. In addition to orbiting around the patient, detectors could be tilted in several different directions through various gimbal mounts. A camera so equipped could theoretically be used for the entire gamut of planar imaging as well as